JOURNAL OF CATALYSIS 127, 512–523 (1991)

Oscillatory Oxidation of CO over Pt at Pressures from 10 to 760 Torr

PATRICIA K. TSAI, MING G. WU, AND M. BRIAN MAPLE

Department of Physics and Institute for Pure and Applied Physical Sciences, University of California at San Diego, San Diego, California 92093

Received October 31, 1988; revised July 30, 1990

Oscillations in the rate of CO oxidation over polycrystalline Pt have been measured at total pressures of 760 and 10 Torr. Despite the pressure change of two orders of magnitude, oscillations occurred between similar values of high and low reactivity, and over roughly the same experimental parameters. The lack of dependence of the reaction kinetics on the pressure is not predicted by the Langmuir–Hinshelwood equations that provide the rate multiplicities underlying the oscillations in a number of recent models. This lack of agreement suggests that the current understanding of CO oxidation and oscillatory reaction kinetics remains incomplete. The primary difference between the oscillations at the two pressures occurred in the waveforms, which were highly structured and fractal-like at $P = 760$ Torr, and became simple square waves on the evolved catalyst surface at $P = 10$ Torr. Differences in the catalyst surface structure and in coupling between parts of the catalyst through concentration gradients in the gas may account for these changes in the complexity of the waveforms.

INTRODUCTION

In earlier work performed in this laboratory, oscillations in the rate of CO oxidation over polycrystalline Pt were systematically studied at atmospheric pressure over a range of experimental parameters (*1*). The oscillations were modeled by Langmuir–Hinshelwood (LH) kinetics with the addition of a driving mechanism involving the slow formation and reduction of a surface oxide species (*2*). Indirect support for this mechanism was provided by thermogravimetric measurements of oxidation and CO-reduction rates (*3, 4*). In addition, Lindstrom and Tsotsis (*5*) have observed oscillations in the intensity of an infrared spectroscopic band that can be identified with CO adsorbed on oxidized Pt (*6*).

In work by Ertl and co-workers, oscillations were observed on Pt(100) at much lower pressures ($\sim 10^{-4}$ Torr) (*7*). Scanning low-energy electron diffraction studies (*8*) demonstrated that the catalyst undergoes periodic surface reconstruction, and the oscillations at these pressures have been modeled (*9*) by LH kinetics with a driving mechanism involving adsorbate-induced transformations between the two surface phases. In addition, surface phase transformations have also been implicated in oscillations on Pt(110) (*10*) and Pt(210) (*11*). No oscillations have been obtained on Pt(111) (*12, 13*) which does not undergo a surface reconstruction. Yeates *et al.* (*13*) have suggested that different mechanisms apply at high and low pressures.

In the first report of oscillations characterized continuously from low to high pressures, Ehsasi *et al.* (*14*) monitored oscillations in the rate of CO oxidation over Pd(110) from 10^{-3} to 1 Torr. The general features of the oscillations were unchanged over this range of pressures, suggesting that a single mechanism is responsible for the oscillations. Reversible surface structural changes can be ruled out because clean Pd(110) does not reconstruct. Subsequent experiments by Ladas *et al.* (*15*) have provided evidence that subsurface oxygen may be involved in these oscillations.

In an effort to explore the pressure gap for Pt catalysts, we have studied oscillations in the rate of CO oxidation on a polycrystal-

0021-9517/91 $3.00

line wire in a reactor capable of continuously variable pressures. In this work we report experimental results for oscillations at total pressures of 760 and 10 Torr. This is the first study in which measurements of the reaction rate can be compared over this range of pressures.

Despite the change in pressure of two orders of magnitude, the rates on the high and low reactivity branches remained the same, and oscillations occurred over roughly the same gas temperatures and gas compositions. In contrast, pressure variations cause large shifts to occur in the Langmuir–Hinshelwood rate multiplicities underlying the oscillations in a number of recently developed theoretical models (*2, 9, 16*). Thus, the LH expressions used in these models do not describe the observed pressure dependence. This lack of agreement indicates that the current understanding of CO oxidation and oscillatory reaction kinetics remains incomplete.

The primary difference between the oscillations at the two pressures occurred in the shapes of the waveforms. These variations suggest that surface structure and coupling through gas phase diffusion influence the complexity of the oscillations. These results support other recent work in which coupling through the gas phase has been shown to occur during oscillations at atmospheric pressure (*17–21*) and low pressures (*22, 23*).

METHODS

The apparatus, shown in Fig. 1, was a bakeable gas flow reactor which could be operated at atmospheric pressure and below. Reactant gases were carbon monoxide (99.99%), oxygen (99.99%), and helium (99.999%). The reactor was a quartz tube with an inner diameter of 22 mm. The pressure P in the reactor was monitored by a capacitance manometer. Additional details regarding the apparatus appear in Ref. (*20*).

A constant mass flow was maintained at a value of 100 cm^3/min of gas at room temperature and atmospheric pressure. With a variable leak valve and a 300 liter/s turbomolecular pump, we were able to decrease the pressure continuously from $P = 760$ Torr to $P \ll 1$ Torr. The oxygen mass flow rate was held constant at half the total mass flow rate, so that the oxygen partial pressure in the reaction mixture was $P_{O_2} = 0.5P$. The gas composition was changed by varying the CO mass flow rate. Helium composed the remainder of the gas stream.

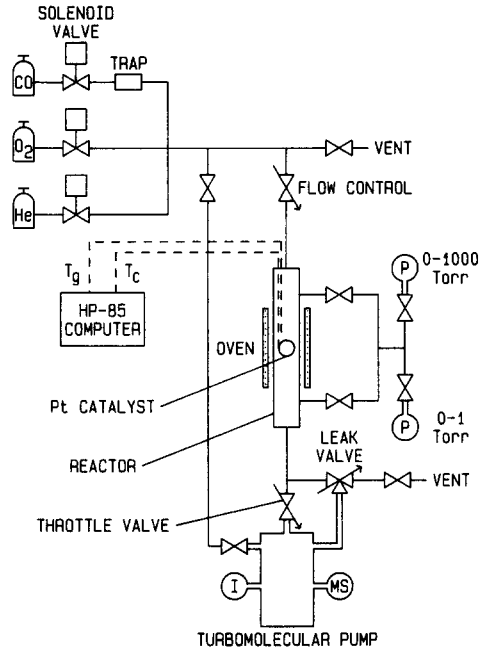

FIG. 1. Gas flow reactor, operated between atmospheric pressure and 10 Torr in these experiments. P: capacitance manometer. I: ion gauge. MS: mass spectrometer.

The catalyst was a polycrystalline Pt wire (99.99%) with a length of 2.5 cm and a diameter of 0.05 cm. The ends of the wire were spotwelded together to form a loop. The loop, which had been used in previous oscillatory experiments, was etched for $\lesssim$1 min in hot aqua regia before use in this work. A thermocouple spotwelded to the wire measured the catalyst temperature, T_c. Another thermocouple situated upstream from the catalyst measured the gas temperature, T_g.

Measurement of Reaction Rates

Because CO oxidation is exothermic, the increase in catalyst temperature over the gas temperature, $\Delta T_c = T_c - T_g$, could be used to measure the reaction rate on the catalyst in the vicinity of the thermocouple. Under our experimental conditions, the measured values of ΔT_c were smaller than the range of gas temperatures over which oscillations occurred for a given gas composition. For example, for $P_{CO}/P_{O_2} = 0.01$, oscillations occurred over a $\gtrsim$60°C range of gas temperatures and had maximum amplitudes of ~10°C.

For flow with low Reynolds numbers (Re $\lesssim$ 1), heat is transferred primarily through conduction (*24*). In our experiments, the Reynolds number for flow around the catalyst wire was $Re_w \sim 0.06$. Since the thermal conductivity of a gas is independent of pressure in the viscous regime (*25*), a given temperature increase ΔT_c corresponds to the same rate of CO_2 production regardless of the pressure.

Oscillations at P = 760 Torr

At atmospheric pressure, oscillations with a fractal-like appearance occurred for all gas compositions studied, $P_{CO}/P_{O_2} = 0.002$ to 0.04. These highly structured, quasiperiodic waveforms were characterized by excursions of varying amplitudes from a state of high reaction rate toward a quenched state, as shown for $P_{CO}/P_{O_2} = 0.01$ in Fig. 2. Some oscillations at lower gas temperatures had fundamental periods as long as 2 or 3 h.

In order to characterize the reaction kinetics as a function of gas temperature, the minimum and maximum reaction rates achieved during a complete oscillatory cycle were measured as T_g was varied slowly for a fixed CO partial pressure. The same qualitative behavior occurred for all gas compositions. In the top portion of Fig. 3, data obtained as T_g was increased at the rate of 10°C/h are plotted as a function of T_g for $P_{CO}/P_{O_2} = 0.01$. Fractal-like oscillations appeared at gas temperatures from 216 to 322°C, where the branches of high and low reactivity overlap. Excellent reproducibility was obtained between successive runs with scan rates from ±1 to ±20°C/h. Over time scales of 1 or 2 weeks, the maximum gas temperature for oscillations varied by ±30°C for a given gas composition.

Oscillations were also monitored as the CO partial pressure was varied for a constant gas temperature. In Fig. 4, the open symbols represent minimum and maximum reaction rates measured as a function of the partial pressure ratio P_{CO}/P_{O_2} for T_g = 294°C. Fractal-like oscillations occurred for P_{CO}/P_{O_2} from 0.005 to 0.035. No hysteresis was observed for increasing and decreasing P_{CO}.

Fourier Analysis of the Time Series at P = 760 Torr

The power spectrum of the oscillations in Fig. 2A is plotted in Fig. 5. Instead of a single fundamental frequency, three closely spaced peaks (the triplet peaks) appear with frequencies ω_1 to ω_3. The corresponding periods, τ_1 to τ_3, are comparable to the "quasiperiods" in Fig. 2A. The amplitudes of the triplet peaks show considerable variation when power spectra of different portions of the time series are taken. However, these peaks occurred at distinct frequencies and were not produced by the drift of a single peak.

A number of higher frequency peaks appear with strong amplitudes in Fig. 5, and two are comparable in amplitude to the triplet peaks. Due to the close spacing of the triplet peaks, all of the higher frequency points can be expressed as integral linear combinations of the triplet peaks, $\omega = \sum_{i=1}^{3} n_i\omega_i$, within $\Delta\omega = 2\pi/T$, (n_i = integer; T = length of time series). However, none of the nine strongest high frequency peaks is a simple harmonic $n_i\omega_i$.

Oscillations at P = 10 Torr

When the pressure was reduced to 10 Torr, the oscillations immediately became much less complex in shape. Initially, the waveforms were somewhat fractal-like, but

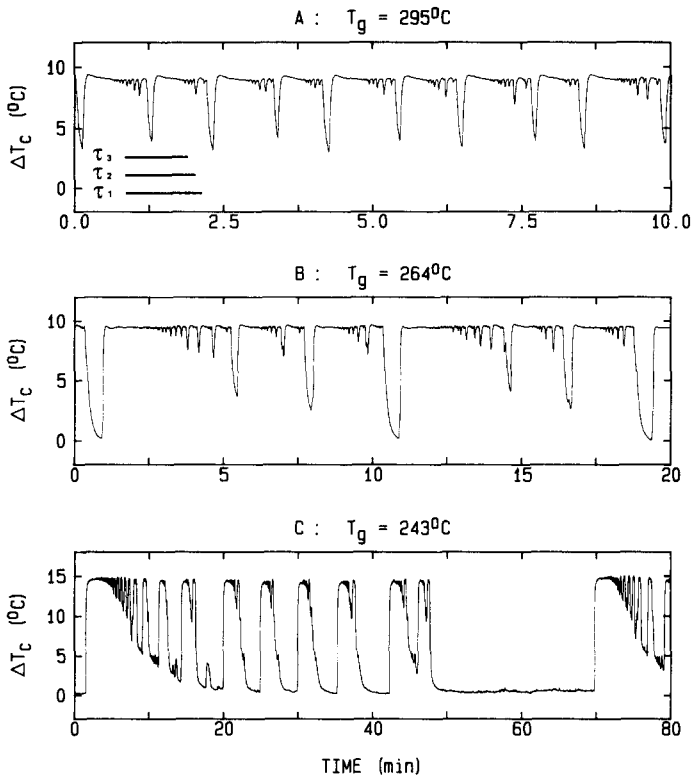

FIG. 2. (A–C) Examples of waveforms during oscillations in the rate of CO oxidation over the Pt loop for various gas temperatures T_g. The partial pressure ratio was $P_{CO}/P_{O_2} = 0.01$; the total pressure was $P = 760$ Torr. The vertical scale gives the temperature difference ΔT_c between the Pt catalyst and the gas. This temperature difference is proportional to the rate of the exothermic reaction. (A) The bars labeled τ_1 to τ_3 are the periods corresponding to the frequency peaks ω_1 to ω_3 in Fig. 5. (C) Maximum reaction rates attained in these oscillations were higher because gas flow rates were double those used in the other figures.

had much less detailed structure than at $P =$ 760 Torr, and oscillatory amplitudes became significant only after pretreatment in the reaction mixture above 350°C. As a result of changes in the catalyst surface, waveforms evolved over several weeks into simple square waves with no dependence on the catalyst pretreatment or the direction of the scan.

Examples of waveforms recorded for $P_{CO}/P_{O_2} = 0.01$ after the oscillatory behavior stabilized are shown in Fig. 6. These square waves are nearly structureless, but agree well in amplitude and period with the oscillations recorded at comparable gas temperatures at atmospheric pressure. In the bottom portion of Fig. 3, minimum and maximum reaction rates measured at $P =$ 10 Torr are plotted for $P_{CO}/P_{O_2} = 0.01$ as T_g was increased at 20°C/h. Square wave oscillations occurred from 250 to 310°C, a somewhat narrower range of gas temperatures than for the fractal-like oscillations at $P = 760$ Torr. For all P_{CO}/P_{O_2} ratios sampled between 0.0025 and 0.04, the minimum T_g at which oscillations occurred was higher (typically by 50–60°C) at $P = 10$ Torr than at atmospheric pressure.

In Fig. 4, reaction rates measured under the conditions $T_g = 294$°C, $P = 10$ Torr are plotted as the closed symbols as a function of the partial pressure ratio P_{CO}/P_{O_2}. Oscillations were present for P_{CO}/P_{O_2} from 0.0075 to 0.02. Despite an interval of 11 weeks between the measurements at $P = 10$ Torr and $P = 760$ Torr, excellent agreement occurred

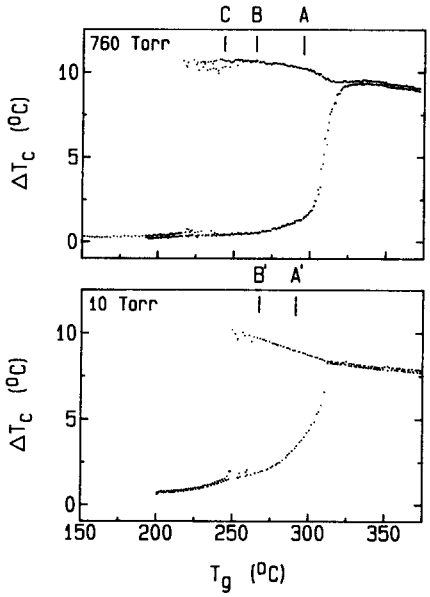

FIG. 3. Bifurcation diagrams showing the gas temperatures at which oscillations were observed at P_{CO}/P_{O_2} = 0.01. Top: At P = 760 Torr, oscillations occurred between 216 and 322°C. A, B, and C show the gas temperatures at which the waveforms in Fig. 2 were recorded. Bottom: At P = 10 Torr, oscillations occurred between 250 and 310°C. A′ and B′ show the gas temperatures at which the waveforms in Fig. 6 were recorded.

between the reaction rates measured at a given P_{CO}/P_{O_2}.

Upon completion of the measurements at P = 10 Torr, the reactor was returned to atmospheric pressure. Fractal-like waveforms reappeared at gas temperatures consistent with previous results.

DISCUSSION

When the pressure in our experiments was changed by two orders of magnitude and the fractional molar composition of the gas remained the same, oscillations occurred between similar values of the catalyst temperature and with similar frequencies over roughly the same ranges of gas temperature. This lack of dependence on the pressure is not predicted by the Langmuir–Hinshelwood mechanism that is used as the starting point for a number of kinetic models for oscillatory CO oxidation. The primary difference between the oscillations at the two pressures occurred in the complexity of the waveforms, which were highly structured and fractal-like at P = 760 Torr, and became simple square waves on the evolved catalyst surface at P = 10 Torr. Differences in the catalyst surface structure and in coupling between parts of the catalyst through concentration gradients in the gas may account for this result.

Reaction Kinetics

The oscillatory reaction rates and periods showed a remarkable lack of dependence on the total pressure for fixed molar gas composition.

For P_{CO}/P_{O_2} = 0.01, the largest increases in catalyst temperature $\Delta T = T_c - T_g$ were 10°C for P = 10 to 760 Torr. The heat transfer equation, which can be used to evaluate the reaction rate R from $T_c - T_g$, yields the result that a given temperature increase corresponds to the same CO_2 production rate regardless of pressure. Briefly,

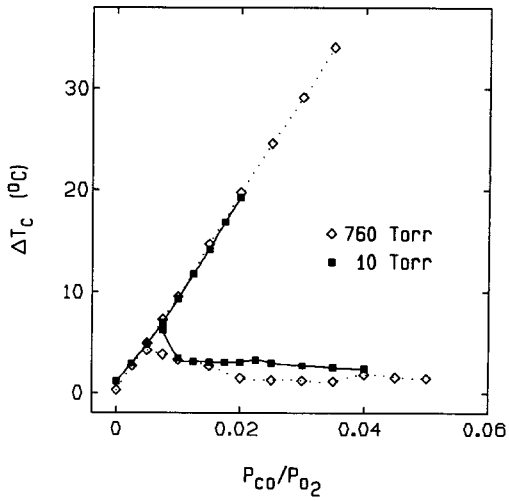

FIG. 4. Bifurcation diagram showing the partial pressure ratios over which oscillations occurred at T_g = 294°C. Open symbols: At P = 760 Torr, oscillations occurred for P_{CO}/P_{O_2} = 0.005 to 0.035. Closed symbols: At P = 10 Torr, oscillations occurred for P_{CO}/P_{O_2} = 0.0075 to 0.02.

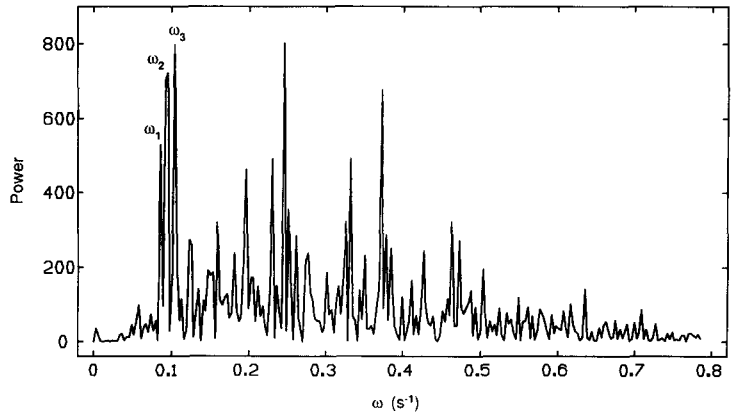

FIG. 5. Power spectrum of the waveform in Fig. 2A. Recorded at intervals of 0.5 s, 4096 points were used in the transform.

$$R = \frac{hA}{(-\Delta H)}(T_c - T_g), \qquad (1)$$

where A is the surface area of the catalyst, and ΔH is the enthalpy change of reaction. The heat transfer coefficient h is given by

$$h = f(\mathrm{Re}, \mathrm{Pr})\frac{k}{d_w}, \qquad (2)$$

where f is a function dependent on the flow geometry, Re is the Reynolds number, Pr is the Prandtl number, k is the thermal conductivity of the gas, and d_w is the diameter of the catalyst wire. Under the conditions of viscous flow and constant throughput maintained in our experiments, the parameters Re, Pr, k, d_w, and consequently h are independent of pressure, so that the reaction rate has the same relationship to the increase in catalyst temperature regardless of pressure. Additional details, including the evaluation of h, appear in the Appendix. For $T_c - T_g = (T_c - T_g)_{max} = 10°C$,

$$R = 7.8 \times 10^{-8} \text{ mol s}^{-1}.$$

The corresponding maximum CO conversion is 23%.

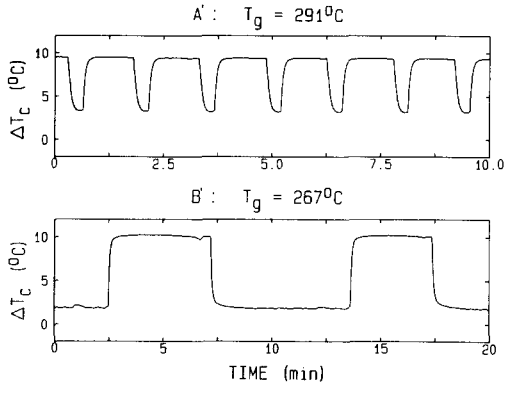

FIG. 6. Waveforms for $P_{CO}/P_{O_2} = 0.01$ after the oscillatory behavior had stabilized at $P = 10$ Torr.

The difference in the CO concentration between the bulk gas and the gas at the catalyst surface, $n_{CO} - n_{CO,s}$, can be estimated for the maximum CO conversion from the reaction rate obtained above and the mass transfer equation:

$$R = 7.8 \times 10^{-8} \text{ mol s}^{-1} = \beta A(n_{CO} - n_{CO,s}). \qquad (3)$$

The mass transfer coefficient β is given by

$$\beta = f(\mathrm{Re}, \mathrm{Sc})\frac{D}{d_w}. \qquad (4)$$

Details regarding the evaluation of β are given in the Appendix. Under our experimental conditions, the Schmidt number Sc is independent of pressure, and the diffusivity of the reactant species D is inversely proportional to the total pressure. Thus,

$\beta \propto 1/P$, and the same difference between the CO partial pressure in the bulk and at the catalyst surface, $P_{CO} - P_{CO,s}$, occurs relative to the total pressure:

$$\frac{P_{CO} - P_{CO,s}}{P} = 0.0028.$$

In our experiments, $P_{CO} = 0.01P$, so that $P_{CO,s} = 0.72P_{CO}$. This result shows that mass transfer gradients, while significant under conditions of maximum conversion, scale with the total pressure. These gradients may limit the measured temperature increases at high conversions but do not affect our conclusions qualitatively.

Thus, a kinetic model of oscillations must yield an expression for the reaction rate that is a function of the mole fractions y_{O_2} and y_{CO} but independent of the total pressure on both reaction branches:

$$R = F\left(\frac{P_{O_2}}{P}, \frac{P_{CO}}{P}\right) = F(y_{O_2}, y_{CO}).$$

While there are limited data allowing direct comparison of oscillations in CO oxidation at varying pressures, other researchers have obtained results similar to ours. Ehsasi *et al.* (*14*) stated that the general features of oscillations in CO oxidation over Pd(110) remained unchanged from $\sim 10^{-3}$ to 1 Torr. Lindstrom and Tsotsis used transmission IR spectroscopy to study steady-state and oscillatory CO oxidation, and found qualitatively similar results at 1–10 Torr (*26*) and at atmospheric pressure (*5*).

CO oxidation rates in the absence of rate multiplicities have been measured at varying pressures over Rh (*27*) and Pd (*28, 29*) catalysts. Rates measured in the regime in which the reaction rate showed a negative-order dependence in P_{CO} for a given P_{O_2} (the CO inhibition regime, corresponding to the branch of low reactivity) were independent of the total pressure when P_{CO}/P_{O_2} was held fixed. Oh *et al.* (*27*) found that CO oxidation rates over Rh/Al_2O_3 in the CO inhibition regime remained virtually the same over a wide range of temperatures as $P_{CO} + P_{O_2}$ was varied from 7.6 to 30 Torr with $P_{CO}/P_{O_2} = 1$. Ladas *et al.* (*28*) studied CO oxidation over supported Pd particles at pressures from 1×10^{-7} to 1.2×10^{-6} Torr. Their rate measurements in the CO inhibition regime showed remarkable agreement with independent measurements by Cant *et al.* (*29*) at ~1 Torr for a ratio of $P_{CO}/P_{O_2} = 2$. In the regime in which the reaction rate showed a positive-order dependence in P_{CO} for a given P_{O_2} (corresponding to the branch of high reactivity), Ladas *et al.* (*28*) found that the rate increased linearly with the total pressure when $P_{CO}/P_{O_2} = 0.91$ was held fixed.

The mechanism for CO oxidation over Pt has been established (*30*) to occur through the elementary reaction steps,

$$O_2 + 2S \xrightarrow{k_1} 2O_{ad} \quad (5)$$

$$CO + S \underset{k_3}{\overset{k_2}{\rightleftharpoons}} CO_{ad} \quad (6)$$

$$CO_{ad} + O_{ad} \xrightarrow{k_{LH}} CO_2, \quad (7)$$

where S denotes a surface site; CO_{ad}, O_{ad} represent chemisorbed species; $k_{1,2,3}$ are the rate constants for O_2 adsorption, CO adsorption, and CO desorption; and k_{LH} is the rate constant for reaction. At the temperatures at which oscillations occur, the desorption of O_2 can be neglected, and CO_2 can be taken to desorb immediately.

For adsorbed reactants randomly distributed over a uniform surface, the rate equations associated with the mechanism above are

$$\frac{d\theta_O}{dt} = k_1 P_{O_2}(1 - \theta_O - \theta_{CO})^2 - k_{LH}\theta_O\theta_{CO} \quad (8)$$

$$\frac{d\theta_{CO}}{dt} = k_2 P_{CO}(1 - \theta_O - \theta_{CO}) - k_{LH}\theta_O\theta_{CO} - k_3\theta_{CO}, \quad (9)$$

where $\theta_{O,CO}$ = fractional surface coverages of chemisorbed O, CO.

While Eqs. (8) and (9) do not predict oscil-

lations, multiple reaction branches appear in their steady-state solutions ($d\theta_O/dt = d\theta_{CO}/dt = 0$) under some conditions in agreement with observations (*1, 31*). As noted by Chang and Aluko (*32*), "the two stable branches of [Eqs. (8) and (9)] are generally regarded as the two states between which the oscillations take place, and the slow mechanism offers the switching mechanism," where the "slow mechanism" (such as surface oxidation) occurs on a time scale long compared to the time scales for chemisorption or the Langmuir–Hinshelwood reaction.

A number of models for CO oxidation over Pt have been developed with different slow mechanisms driving the oscillations, including the formation and removal of an oxide (*2*) or carbon (*16*) species, and adsorbate-induced surface reconstruction (*9*). The Langmuir–Hinshelwood mechanism outlined above provides the rate multiplicities underlying the oscillations in all these models. Thus, the behavior of the stable steady states predicted by Eqs. (8) and (9) provides a test for the applicability of the Langmuir–Hinshelwood mechanism used in these models with respect to changes in the pressure.

On the branch of high reactivity, the reaction rate is large compared to the CO desorption rate ($k_{LH}\theta_O\theta_{CO} \gg k_3\theta_{CO}$), so that

$$k_1P_{O_2}(1 - \theta_O - \theta_{CO})^2 - k_{LH}\theta_O\theta_{CO} = 0 \quad (10)$$

$$k_2P_{CO}(1 - \theta_O - \theta_{CO}) - k_{LH}\theta_O\theta_{CO} \approx 0. \quad (11)$$

Combining Eqs. (10) and (11) yields

$$R_{LH} \approx \frac{(k_2P_{CO})^2}{k_1P_{O_2}}. \quad (12)$$

In our experiments, P_{CO}/P_{O_2} was held fixed, and the total pressure was varied. Under these conditions, Eq. (12) would predict $R_{LH} \propto P_{CO}$, in contrast with our experimental results.

On the branch of low reactivity, the reaction rate is inhibited by a large CO coverage ($k_3\theta_{CO} \gg k_{LH}\theta_O\theta_{CO}$), so that

$$k_1P_{O_2}(1 - \theta_O - \theta_{CO})^2 - k_{LH}\theta_O\theta_{CO} = 0 \quad (13)$$

$$k_2P_{CO}(1 - \theta_O - \theta_{CO}) - k_3\theta_{CO} \approx 0. \quad (14)$$

Combining Eqs. (13) and (14) yields

$$R_{LH} \approx \frac{k_1P_{O_2}}{\left(1 + \frac{k_2P_{CO}}{k_3}\right)^2}. \quad (15)$$

Again, this prediction does not agree with our experimental results. Thus, the Langmuir–Hinshelwood mechanism as defined in Eqs. (8) and (9) does not describe the observed pressure dependence.

The oxide model consists of Eqs. (8) and (9) with the addition of another equation and terms corresponding to the formation and reduction of an oxide species:

$$\frac{d\theta_O}{dt} = k_1P_{O_2}(1 - \theta_O - \theta_{CO} - \theta_{ox})^2 - k_{LH}\theta_O\theta_{CO} \quad (16)$$

$$\frac{d\theta_{CO}}{dt} = k_2P_{CO}(1 - \theta_O - \theta_{CO} - \theta_{ox}) - k_{LH}\theta_O\theta_{CO} - k_3\theta_{CO} \quad (17)$$

$$\frac{d\theta_{ox}}{dt} = k_{ox}\theta_O(1 - \theta_O - \theta_{CO} - \theta_{ox}) - k_{red}\theta_{ox}\theta_{CO}. \quad (18)$$

Reaction rates computed from Eqs. (16)–(18) with an integrating routine for stiff differential equations exhibit the same pressure dependence as the rates R_{LH} in Eqs. (12) and (15) derived from the steady-state Langmuir–Hinshelwood mechanism. The contrast between these predictions and our experimental results shows the need for further studies in the "pressure gap."

We note that Oh *et al.* (*28*) successfully modeled their data for CO oxidation over Rh/Al_2O_3 with oxygen adsorption described by a first-order term, $k_1P_{O_2}(1 - \theta_O - \theta_{CO})$, instead of the squared term, $k_1P_{O_2}(1 - \theta_O - \theta_{CO})^2$, in Eq. (8). Under conditions approaching the CO adsorption–desorption equilibrium, corresponding to the low reactivity branch, the reaction rate depends only on the ratio of reactant partial pressures,

P_{CO}/P_{O_2}, and not on the total pressure. However, rate multiplicities do not exist in their linearized model. Moreover, the desired dependence on the ratio of partial pressures applies only to the low reactivity branch. Thus, their model does not suitably describe the steady-state kinetics underlying oscillatory behavior.

Complexity of Waveforms

The primary difference between the oscillations at the two pressures lies in the complexity of the waveforms. The highly structured character of the fractal-like oscillations in Fig. 2 suggests the development of cooperative behavior between a large number of individually active portions of the catalyst surface. This idea is supported by Fig. 5, in which a number of frequencies are required to characterize the power spectrum.

Fractal-like oscillations appeared in one of the earliest accounts of CO oxidation over supported Pt (*33*), and have occurred in a variety of catalytic reactions (*34, 35*). Recently, observations of fractal-like oscillations in CO oxidation over supported Pd by Jaeger *et al.* (*36, 37*) have been qualitatively reproduced by a cellular automaton model (*36, 38–40*) in which the collective behavior of crystallites in a two-dimensional array is synchronized by local interaction. The power spectra (*40*) are characterized by a number of independent frequencies in a similar fashion to the power spectrum in Fig. 5. The low thermal conductivity of the support and the result that oscillations were not significantly affected by changes in the thermal contact between catalyst pellets led Jaeger *et al.* (*36, 37*) to conclude that heat transfer is not the mechanism synchronizing oscillations. Rather, they proposed that small gradients in the gas phase concentrations propagate from trigger locations across the catalyst surface, resulting in the development of highly complex oscillations. This idea was supported by experiments in which periodic variations in the CO feed concentration caused aperiodic oscillations to become synchronized with the forcing signal (*41*).

When we lowered the pressure to 10 Torr, the oscillations initially retained some of their fractal-like character but decreased significantly in complexity. Over a period of several weeks, the oscillations evolved into the simple square waves in Fig. 6. Both the immediate change in the waveforms and their gradual evolution are consistent with the change in the gas phase diffusivity D, which varies inversely with pressure. At 760 Torr, the diffusion time across the loop is $\Delta t = d^2/D \sim 1$ s, where $d = 0.8$ cm is the diameter of the loop, and $D = 0.7$ cm^{2}s^{-1} is the mutual diffusion coefficient of CO and O_2 at 200°C (*25*). The time Δt is comparable to the time scales corresponding to the smallest amplitude fluctuations resolvable in the oscillations at this pressure. At 10 Torr, the diffusion time across the loop is $\Delta t \sim 0.01$ s, and small fluctuations on either reaction rate branch were beyond our sampling frequency.

Our results suggest that complex waveforms occurred at 760 Torr because the catalyst surface consisted of individually active areas which were stable under the reaction conditions and which coupled through gas phase diffusion. When the pressure was reduced to 10 Torr, communication increased between the active areas, and the fractal-like aspect of the waveforms decreased. Under the reaction conditions at 10 Torr, the catalyst surface gradually evolved, and the increased rate of coupling through the gas enabled the entire loop to oscillate in synchrony.

Two studies using recycle reactors have also shown that gas phase coupling plays a role in the synchronization of oscillations during CO oxidation over supported catalysts. In a study with a supported Pt–Pd catalyst, Lynch and Wanke (*17*) found that waveforms became simpler as the recycle ratio was increased. More recently, Kapicka and Marek (*21*) found that decreasing the recycle ratio resulted in the desynchro-

nization of oscillations monitored by thermocouples embedded in five supported Pt pellets in a packed bed.

In work by Ertl and co-workers (*8, 9*), coupling between surface reaction and surface diffusion led to propagation of phase transformations across a Pt(100) single crystal. Complex oscillations propagated from imperfections in the surface structure near the edge of the crystal. In contrast, regular and reproducible oscillations occurred on Pt(110) (*10*). No spatial structures were detected, indicating that spatial organization occurred through feedback through the gas phase. Eiswirth *et al.* (*42*) attributed this difference in the complexity of the oscillations to differences in the sensitivity of the two crystal planes to small variations in the partial pressures.

Synchronization of catalytic activity through gas phase diffusion may account for the differences between two experiments using spatially resolved Fourier-transform infrared spectroscopy to study CO oxidation on supported Pt wafers. Working at atmospheric pressure, Kaul and Wolf (*43*) observed differences in the waveforms on the four quadrants of their wafers. In contrast, Lindstrom and Tsotsis (*44*) found that oscillations on the four quadrants of their catalysts occurred in phase with each other at 2–10 Torr.

Finally, we note that the fractal-like oscillations at 760 Torr occurred at lower gas temperatures than the simple oscillations at 10 Torr. This result is consistent with conclusions obtained in earlier work (*20*) in which we found that coupling between individually active areas can cause complex oscillations to occur at lower temperatures than on a catalyst that is oscillating in synchrony.

APPENDIX

We derive the pressure dependence of the heat and mass transfer coefficients and discuss their evaluation.

The heat transfer coefficient h is defined by Eq. (1) in the text. Dimensional analysis suggests a related dimensionless form, the so-called Nusselt number Nu (*45*),

$$\mathrm{Nu} = \frac{hd}{k} = f(\mathrm{Re}, \mathrm{Pr}), \qquad (19)$$

where

d = catalyst dimension
k = thermal conductivity of gas
Re = Reynolds number
Pr = Prandtl number.

The function f is dependent on the flow geometry, and is in general empirically determined. Rearranging terms in Eq. (19) yields Eq. (2):

$$h = f(\mathrm{Re}, \mathrm{Pr})\frac{k}{d}.$$

In order to determine the pressure dependence of h, it is necessary to examine the pressure dependence of k, Re, and Pr,

$$\mathrm{Re} = \frac{d\rho u}{\mu}$$

$$\mathrm{Pr} = \frac{\mu c_p}{k},$$

where

ρ = gas density
u = linear velocity of the gas stream
μ = gas viscosity
c_p = specific heat of gas.

In the viscous regime ($P > 10^{-3}$ Torr), k, μ, and c_p are independent of pressure (*25*). In our experiments, a constant mass flow per cross-sectional area ρu was maintained when the pressure was changed. Thus, h is independent of pressure, as stated in the text.

Similarly, the mass transfer coefficient β is defined by Eq. (3) in the text. Dimensional analysis leads to the dimensionless Sherwood number (*45*)

$$\mathrm{Sh} = \frac{\beta d}{D} = f(\mathrm{Re}, \mathrm{Sc}), \qquad (20)$$

where

D = diffusivity of reactant species

Sc = Schmidt number $= \frac{\mu}{\rho D}$.

As discussed in Ref. (*45*), for the same geometry, $f(\mathrm{Re}, \mathrm{Sc})$ in Eq. (20) has the same functional form as $f(\mathrm{Re}, \mathrm{Pr})$ in Eq. (19). Rearranging terms in Eq. (20) yields Eq. (4):

$$\beta = f(\mathrm{Re}, \mathrm{Sc})\frac{D}{d}.$$

In the viscous regime, $\rho \propto P$, and $D \propto 1/P$ (*25*), so Sc is independent of pressure. Previously we showed that under the conditions of our experiment Re is independent of pressure. Thus, the pressure dependence of β is determined by the pressure dependence of D:

$$\beta \propto \frac{1}{P}.$$

The heat and mass transfer coefficients were evaluated using Eqs. (2) and (4) and the function $f(\mathrm{Re}, x)$ for heat transfer (x = Pr) or mass transfer (x = Sc) for a long cylinder of diameter equal to our wire diameter (*46*):

$$f(\mathrm{Re}, x) = 0.989\mathrm{Re}^{0.330}x^{1/3}.$$

Substituting values at 200°C from our experiments we obtain

$$h = 8.3 \times 10^{-3}\,\mathrm{Jcm^{-2}s^{-1}K^{-1}};$$

$$\beta = 6.4 \times 10^{-2}\,\mathrm{ms^{-1}} \quad \text{at } P = 760\,\mathrm{Torr};$$

$$\beta = 4.9\,\mathrm{ms^{-1}} \quad \text{at } P = 10\,\mathrm{Torr}.$$

ACKNOWLEDGMENTS

We are grateful to Richard K. Herz for stimulating discussions on the interpretation of our results. This work was supported by the U.S. Department of Energy under Contract DE-AT03-76ER70227.

REFERENCES

1. Turner, J. E., Sales, B. C., and Maple, M. B., *Surf. Sci.* **103,** 54 (1981).
2. Sales, B. C., Turner, J. E., and Maple, M. B., *Surf. Sci.* **114,** 381 (1982).
3. Sales, B. C., Turner, J. E., and Maple, M. B., *Surf. Sci.* **112,** 272 (1981).
4. Turner, J. E., and Maple, M. B., *Surf. Sci.* **147,** 647 (1984).
5. Lindstrom, T. H., and Tsotsis, T. T., *Surf. Sci.* **150,** 487 (1985).
6. Herz, R. K., and Shinouskis, E. J., *Appl. Surf. Sci.* **19,** 373 (1984).
7. Ertl, G., Norton, P. R., and Rustig, J., *Phys. Rev. Lett.* **49,** 177 (1982).
8. Cox, M. P., Ertl, G., and Imbihl, R., *Phys. Rev. Lett.* **54,** 1725 (1985).
9. Imbihl, R., Cox, M. P., Ertl, G., Muller, H., and Brenig, W., *J. Chem. Phys.* **83,** 1578 (1985).
10. Eiswirth, M., and Ertl, G., *Surf. Sci.* **177,** 90 (1986).
11. Ehsasi, M., Block, J. H., Christmann, K., and Hirschwald, W., *J. Vac. Sci. Technol. A* **5,** 821 (1987).
12. Norton, P. R., Bindner, P. E., Griffiths, K., Jackman, T. E., Davies, J. A., and Rustig, J., *J. Chem. Phys.* **80,** 3859 (1984).
13. Yeates, R. C., Turner, J. E., Gellman, A. J., and Somorjai, G. A., *Surf. Sci.* **149,** 175 (1985).
14. Ehsasi, M., Seidel, C., Ruppender, H., Drachsel, W., Block, J. H., and Christmann, K., *Surf. Sci.* **210,** L198 (1989).
15. Ladas, S., Imbihl, R., and Ertl, G., *Surf. Sci.* **219,** 88 (1989).
16. Collins, N. A., Sundaresan, S., and Chabal, Y. J., *Surf. Sci.* **180,** 136 (1987).
17. Lynch, D. T., and Wanke, S. E., *J. Catal.* **88,** 345 (1984).
18. Capsaskis, S. C., and Kenney, C. N., *J. Phys. Chem.* **90,** 4631 (1986).
19. Yentekakis, I. V., Neophytides, S., and Vayenas, C. G., *J. Catal.* **111,** 152 (1988).
20. Tsai, P. K., Maple, M. B., and Herz, R. K., *J. Catal.* **113,** 453 (1988).
21. Kapicka, J., and Marek, M., *J. Catal.* **119,** 508 (1989).
22. Eiswirth, M., and Ertl, G., *Phys. Rev. Lett.* **60,** 1526 (1988).
23. Imbihl, R., Ladas, S., and Ertl, G., *Surf. Sci.* **215,** L307 (1989).
24. Kreith, F., and Bohn, M. S., "Principles of Heat Transfer," 4th ed., p. 350. Harper and Row, New York (1986).
25. Present, R. D., "Kinetic Theory of Gases." McGraw–Hill, New York (1958).
26. Lindstrom, T. H., and Tsotsis, T. T., *Surf. Sci.* **167,** L194 (1986).
27. Oh, S. H., Fisher, G. B., Carpenter, J. E., and Goodman, D. W., *J. Catal.* **100,** 360 (1986).
28. Ladas, S., Poppa, H., and Boudart, M., *Surf. Sci.* **102,** 151 (1981).
29. Cant, N. W., Hicks, P. C., and Lennon, B. S., *J. Catal.* **54,** 372 (1978).
30. Engel, T., and Ertl, G., *Adv. Catal.* **28,** 1 (1979).

31. Herz, R. K., and Marin, S. P., *J. Catal.* **65,** 281 (1980).
32. Chang, H.-C. and Aluko, M., *Chem. Eng. Sci.* **39,** 37 (1984).
33. Beusch, H., Fieguth, P., and Wicke, E., *Adv. Chem. Ser.* **109,** 615 (1972).
34. Gray, P., Griffiths, J. F., and Rogerson, J. S., *in* "Joint ASME/AIChE 18th National Heat Transfer Conference, San Diego, CA 1979."
35. Kurtanjek, Z., Sheintuch, M., and Luss, D., *J. Catal.* **66,** 11 (1980).
36. Jaeger, N. I., Moller, K., and Plath, P. J., *Ber. Bunsenges. Phys. Chem.* **89,** 633 (1985).
37. Jaeger, N. I., Moller, K., and Plath, P. J., *J. Chem. Soc. Faraday Trans. 1* **82,** 3315 (1986).
38. Dress, A. W. M., Gerhardt, M., Jaeger, N. I., Plath, P. J., and Schuster, H., *in* "Temporal Order" (L. Rensing and N. I. Jaeger, Eds.), p. 67. Springer-Verlag, Berlin (1985).
39. Dress, A. W. M., Gerhardt, M., and Schuster, H., *in* "From Chemical to Biological Organization" (M. Markus, S. Muller, and G. Nicolis, Eds.), p. 134. Springer-Verlag, Berlin (1988).
40. Plath, P. J., Moller, K., and Jaeger, N. I., *J. Chem. Soc. Faraday Trans. 1* **84,** 1751 (1988).
41. Svensson, P., Jaeger, N. I., and Plath, P. J., *J. Phys. Chem.* **92,** 1882 (1988).
42. Eiswirth, M., Moller, P., Wetzl, K., Imbihl, R., and Ertl, G., *J. Chem. Phys.* **90,** 510 (1989).
43. Kaul, D. J., and Wolf, E. E., *J. Catal.* **91,** 216 (1985).
44. Lindstrom, T. H., and Tsotsis, T. T., *Surf. Sci.* **167,** L194 (1986).
45. Eckert, E. R. G., and Drake, R. M., "Analysis of Heat and Mass Transfer," Chaps. 7 and 22. McGraw–Hill, New York (1972).
46. Wolf, H., "Heat Transfer," p. 265. Harper and Row, New York (1983).